Electron Cross-Field Transport in a Miniaturized Cylindrical Hall Thruster

Artem N. Smirnov, *Student Member, IEEE*, Yevgeny Raitses, and Nathaniel J. Fisch

Invited Paper

***Abstract*—Conventional annular Hall thrusters become inefficient when scaled to low power. Cylindrical Hall thrusters, which have lower surface-to-volume ratio, are more promising for scaling down. They presently exhibit performance comparable with conventional annular Hall thrusters. The present paper gives a review of the experimental and numerical investigations of electron cross-field transport in the 2.6-cm miniaturized cylindrical Hall thruster (100-W power level). We show that, in order to explain the discharge current observed for the typical operating conditions, the electron anomalous collision frequency ν_B has to be on the order of the Bohm value, $\nu_B \approx \omega_c/16$. The contribution of electron-wall collisions to cross-field transport is found to be insignificant. The optimal regimes of thruster operation at low background pressure (below 10^{-5} torr) in the vacuum tank appear to be different from those at higher pressure ($\sim 10^{-4}$ torr).**

***Index Terms*—Bohm diffusion, electron transport, Hall discharge, Langmuir probes, plasma propulsion, turbulence.**

I. Introduction

THE Hall thruster [1] is a well-studied electric propulsion device at intermediate to high power, but it appears to be promising also for relatively low-power propulsion on near-earth missions [2], such as orbit transfer and repositioning. In a conventional Hall thruster, the plasma discharge is sustained in the axial electric $(\mathbf{E})$ and radial magnetic $(\mathbf{B})$ fields applied in an annular channel. The magnetic field is large enough to lock the electrons in the azimuthal $\mathbf{E} \times \mathbf{B}$ drift, but small enough to leave the ion trajectories almost unaffected. A large fraction of the discharge electrons is emitted by an external cathode. Electron cross-field diffusion provides the necessary current to sustain the discharge. The thrust is generated in reaction to the axial electrostatic acceleration of ions. Ions are accelerated in a quasi-neutral plasma, so that no space-charge limitation is imposed on the achievable current and thrust densities. Conventional Hall thrusters designed for operation in 600–1000 W power range have outer channel diameter about 10 cm, maximal value of the magnetic field about 100–200 G, and applied discharge voltage $U_d = 300$ V.

Manuscript received September 21, 2005. This work was supported in part by a grant from the Air Force Office of Scientific Research, in part by a grant from the Defense Advanced Research Projects Agency (DARPA), and in part by the U.S. Department of Energy under Contract AC02-76CH0-3073.

The authors are with the Princeton University Plasma Physics Laboratory, Princeton, NJ 08543 USA (e-mail: asmirnov@pppl.gov).

Digital Object Identifier 10.1109/TPS.2006.872185

The thruster efficiency is defined as $\eta = T^2/2\mu P$, where T is the generated thrust, μ is the supplied propellant flow rate, and P is the applied electric power. The efficiency of the state-of-the-art kilowatt and subkilowatt conventional Hall thrusters is about 50%–60% [1], [3]. The efficiency can be conveniently factorized as

$$\eta \approx \frac{I_i M}{e\mu} \times \frac{I_i}{I_i + I_e} \times \alpha \tag{1}$$

where M is a mass of a propellant gas atom, e is the electron charge, I_i and I_e are the electron and ion currents, respectively, and α is the efficiency of ion acceleration. The first fraction in the right-hand side of (1), the so-called propellant utilization, is a measure of how effectively the supplied propellant gas is ionized in the discharge, whereas the second fraction, the so-called current utilization, determines how effectively the electron transport to the anode is suppressed by the applied magnetic field. With all other parameters held constant, the thruster efficiency decreases with increasing electron current. Understanding of the mechanisms of electron transport in the discharge is, therefore, essential for the development of higher efficiency thrusters.

The electrons in Hall thrusters exhibit anomalous cross-field transport. The electron conductivity across the magnetic field is larger than that predicted by the classical electron–atom collision rate [1], [4]. It is believed that two collisional processes contribute to the conductivity enhancement in Hall thrusters: 1) electron scattering in electric field fluctuations (anomalous or "Bohm" diffusion [4]), and 2) the electron-wall collisions (the near-wall conductivity [5], [6]). The electron-wall interaction plays also a very important role by shaping the electron distribution function (EDF) in the thruster channel. In Hall discharge simulations, in order to account for an enhanced electron cross-field transport, the two nonclassical conductivity mechanisms are usually incorporated in models in one or another parametric way. In fluid and hybrid fluid-particle models, some investigators impose the anomalous Bohm conductivity inside the channel [7]–[9], while others use only the near-wall conductivity [10] or a combination of both Bohm transport and wall collisions [8]–[16]. Full particle-in-cell (PIC) simulations [17], [18] reveal turbulence increasing the cross-field transport. Some theoretical studies [19], [20] suggest that due to the non-Maxwellian shape of the EDF in a Hall thruster, electron–wall collisions do not make a significant contribution

to cross-field transport. In a 2-kW Hall thruster operated at low discharge voltage [21], in the channel region where the magnetic field was the strongest, anomalous fluctuation-enhanced diffusion was identified as the main mechanism of electron cross-field transport. It is important to emphasize here that most of investigations, which addressed the question of the electron conductivity, have been performed for kilowatt and subkilowatt thrusters, where the maximal magnetic field strength in the channel is about 100–200 G.

Scaling to low-power Hall thrusters requires a thruster channel size to be decreased while the magnetic field must be increased inversely to the scaling factor [1]. Thus, in general, the rate of electron cross-field transport required to sustain the discharge in a low-power thruster may be different from that in kilowatt thrusters. In other types of low-temperature magnetized laboratory plasmas, variation of the electron cross-field diffusion rate with applied magnetic field B occurs indeed. For example, in [22], cross-field diffusion coefficient $D_\perp$ was observed to approach the Bohm value when B was greater than 2–3 kG, while in $B < 1$ kG case $D_\perp$ was much smaller than the Bohm value.

Increasing the magnetic field while the thruster channel sizes are being reduced is technically challenging because of magnetic saturation in the miniaturized inner parts of the magnetic core. A linear scaling down of the magnetic circuit leaves almost no room for magnetic poles or for heat shields, making difficult the achievement of the optimal magnetic fields. Nonoptimal magnetic fields result in enhanced electron transport, power and ion losses, heating and erosion of the thruster parts, particularly the critical inner parts of the coaxial channel and magnetic circuit.

Currently existing low-power Hall thruster laboratory prototypes with channel diameters 2–4 cm operate at 100–300 W power levels with efficiencies in the range of 10%–40% [2]. However, further scaling of the conventional geometry Hall thruster down to sub-centimeter size results in even lower efficiencies, 6% at power level of about 100 W [23]. The low efficiency might arise from a large axial electron current, enhanced by magnetic field degradation due to excessive heating of the thruster magnets, or from a low degree of propellant ionization. Thus, miniaturizing the conventional annular Hall thruster does not appear to be straightforward.

A cylindrical Hall thruster (CHT), illustrated in Fig. 1(a), overcomes these miniaturization problems [24]. It has been studied both experimentally and theoretically [25]–[28]. The thruster consists of a boron-nitride ceramic channel, an annular anode, which serves also as a gas distributor, two electromagnetic coils, and a magnetic core. The axial electron current in a CHT can be reduced by the magnetic field with an enhanced radial component and/or by the strong magnetic mirror in the cylindrical part of the channel. The magnetic field lines intersect the ceramic channel walls. The electron drifts are closed, with the magnetic field lines forming equipotential surfaces, with $E = -\nu_e \times B$. Ion thrust is generated by the axial component of the Lorentz force, proportional to the radial magnetic field and the azimuthal electron current.

The cylindrical channel features a short annular region and a longer cylindrical region. The length of the annular region is selected to be approximately equal to an ionization mean free path of a neutral atom. Compared to a conventional geometry (annular) Hall thruster, the CHT has lower surface-to-volume ratio and, therefore, potentially smaller wall losses in the channel. Having potentially smaller wall losses in the channel, a CHT should suffer lower erosion and heating of the thruster parts, particularly the critical inner parts of the channel and magnetic circuit. This makes the concept of a CHT promising for low-power applications.

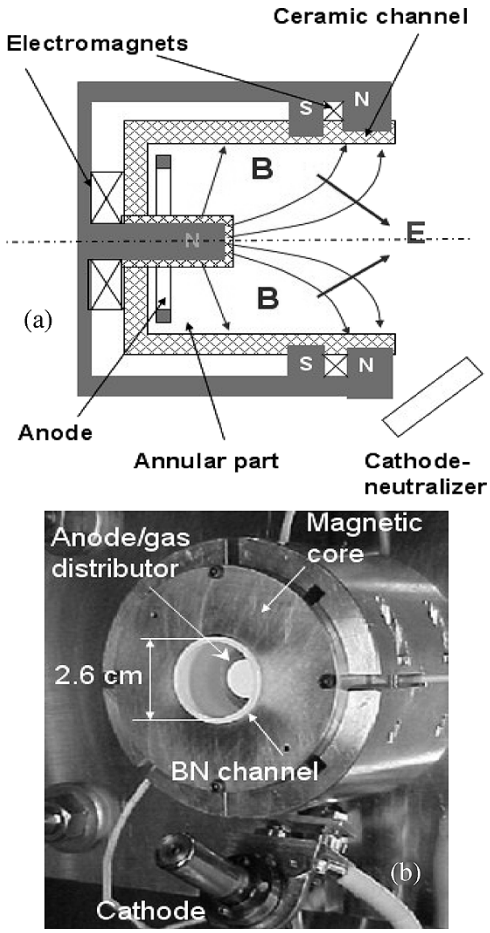

Fig. 1. (a) Schematic of a cylindrical Hall thruster. (b) 2.6-cm cylindrical Hall thruster.

In contrast to the conventional annular geometry, in the cylindrical geometry, the axial potential distribution is critical for electron confinement. This is because there is now a large axial gradient to the magnetic field over the cylindrical part of the channel, which means that electrons drift outwards through the $\mu_e \nabla B$ force, even as they drift azimuthally around the cylinder axis. In the absence of an axial potential, the electrons would simply mirror out of the region of high magnetic field. The axial potential that accelerates ions outwards, now also plays an important role in confining electrons within the thruster.

A relatively large 9-cm-diameter version of the cylindrical thruster, operated in the subkilowatt power range [24], and miniaturized 2.6-cm- [25] and 3-cm-diameter CHTs [29], [30], operated in the power range 50–300 W, exhibit performance comparable with that of the conventional state-of-the-art annular Hall thrusters of the same size. In [27], the plasma

potential, electron temperature, and plasma density distributions were measured inside the 2.6-cm CHT. It was found that even though the radial component of the magnetic field has a maximum inside the annular part of the CHT, the larger fraction of the applied voltage is localized in the cylindrical region. A significant potential drop was also observed in the plume. Ion acceleration in the CHT is expected to occur predominantly in the longitudinal direction and toward the thruster axis. Therefore, the CHT, having lower surface-to-volume ratio as compared with conventional Hall thrusters, may suffer lower erosion of the channel walls and have a longer lifetime.

In recent work [28], electron cross-field transport in a 2.6-cm miniaturized cylindrical Hall thruster was studied through the analysis of experimental data and Monte Carlo (MC) simulations of electron dynamics in the thruster channel. The numerical model takes into account elastic and inelastic electron collisions with atoms, electron–wall collisions, including secondary electron emission, and Bohm diffusion. It was shown that in the typical operating regime, the electron anomalous collision frequency ν_B was of the order of the Bohm value, $\nu_B \approx \omega_c/16$. The contribution of electron–wall collisions to cross-field transport was found to be insignificant.

The present paper gives a review of the experimental and numerical investigations of electron cross-field transport in the 2.6-cm CHT and reports a few recent experimental results that suggest directions for further studies.

This article is organized as follows. In Section II, the main features of the 2.6-cm CHT are presented and the experimental results, obtained in the vacuum facility with a relatively high background pressure, are reviewed. Section III gives a description of the developed MC code and outlines the key results of the numerical simulations. We discuss the electron cross-field transport in Section IV. In Section V, a few recent experimental results, obtained at low background pressure, are presented, and their implications are discussed. In Section VI, we summarize our main conclusions.

II. Experiments

The results of comprehensive experimental investigations of the 2.6-cm CHT are given in [25]–[29]. Experiments described in this section were performed in the Small Hall Thruster facility at Princeton Plasma Physics Laboratory (PPPL), Princeton, NJ.

The 2.6-cm CHT, shown in Fig. 1(b), was scaled down from the 9-cm CHT to operate at about 200-W power level. The total length of the channel is 2.2 cm, the annular region is approximately 0.6 cm long. The outer and the inner diameters of the channel are 2.6 and 1.4 cm, respectively. The overall diameter and the thruster length are both 7 cm.

The magnetic field profiles in the 2.6-cm CHT are shown in Fig. 2(a). The radial component B_r of the magnetic field reaches its maximum near the anode and then reduces toward the channel exit. Although the axial component B_z is also strong, the magnetic field in the annular part of the channel is predominantly radial, the average angle between the field line and the normal to the walls is about 30° [see Fig. 2(b)]. Magnetic field has a mirror-type structure near the thruster axis, with the maximum $\mathrm{B} \sim 1400$ G at the central ceramic piece wall. Due to the

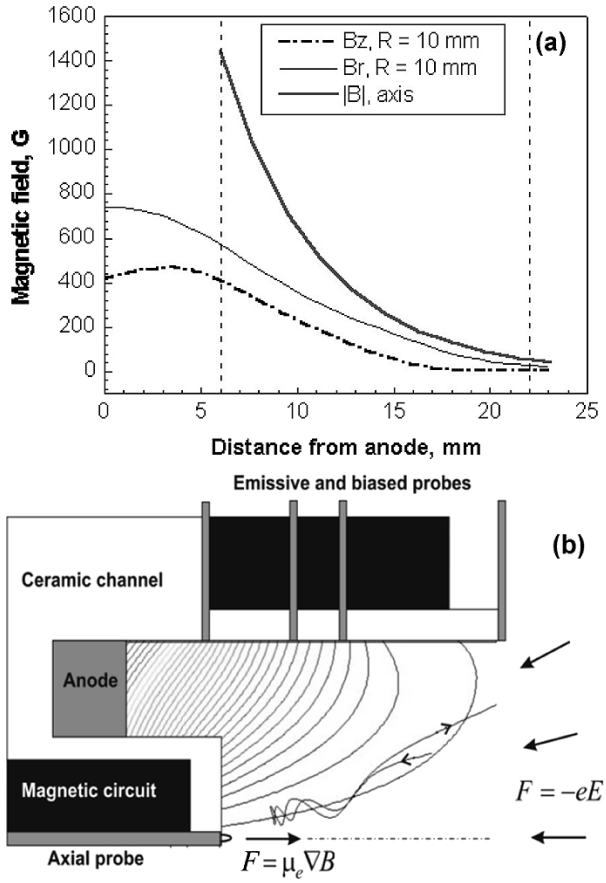

Fig. 2. (a) Magnetic field profiles in the 2.6-cm CHT. $I_{\mathrm{back}} = 2.5$ A, $I_{\mathrm{front}} = -1$ A. Dashed lines at $z = 6$ mm and $z = 22$ mm show the edge of the annular channel part and the thruster exit, respectively. (b) Probe setup used in the experiments. Magnetic field distribution is given for the same coil currents as in Fig. 2(a). Illustrative electron trajectory in the cylindrical part of the channel is indicated, and hybrid mechanism of electron trapping is schematically shown. μ_e is the electron magnetic moment.

mirroring effect of the magnetic field in the cylindrical part of the channel [see Fig. 2(b)], most of the electrons injected from the cathode are reflected from the region of strong B field, and move in the downstream direction. Upon crossing the thruster exit plane and entering the plume plasma, the electrons become unmagnetized and face the potential drop of about 100 V, which reflects them back into the thruster. Thus, most of the electrons injected from the cathode to the CHT appear to be confined in a hybrid trap formed by the magnetic mirror and by the plume potential drop. Diffusion of these electrons across the magnetic field occurs on a time scale much larger than the bounce time in the trap [28].

The typical discharge parameters for the 2.6-cm CHT are: Xe flow rate $\mu = 0.4$ mg/s, discharge voltage $U_d = 250$ V, discharge current $I_d \approx 0.6$ A. Under such conditions, the background gas pressure in the PPPL Small Hall Thruster facility is about 7×10^{-5} torr, the propellant utilization in the 2.6-cm CHT is about 1, and the current utilization is approximately equal to 0.5 [25]. In practice, for the given propellant flow rate, discharge voltage, and background gas pressure, the discharge current is minimized by varying the currents in the magnetic coils. This procedure, which appears to be customary for the annular thrusters, is based on the assumption that near the discharge

current minimum, the variation of the magnetic field affects mainly the electron current to the anode but not the ion current. Thus, the thruster efficiency is maximized by decreasing the discharge current while keeping the generated thrust nearly constant. As shown in Section V, this approach is valid for the CHTs operated at a low background gas pressure (in the 10^{-6} torr range). However, in the relatively high background pressure of the Small Hall Thruster facility ($\sim 10^{-4}$ torr), the reduction of the discharge current in certain magnetic field configurations may be due to the suppression of the background gas ionization. Nonetheless, the operating regime considered in Section II–IV is a typical one for the vacuum environment of the Small Hall Thruster facility.

The distribution of plasma potential ϕ, electron temperature T_e, and plasma density N_e inside the 2.6-cm CHT was studied by means of stationary and movable floating emissive and biased Langmuir probes [28]. The probe setup used in the experiments is shown in Fig. 2(b). Measurements were done at the outer channel wall (at four axial locations: $z = 5$, 10.3, 13.5, and 22 mm), as well as at the thruster axis. The results of the probe measurements are shown in Fig. 3. The potential drop in the 2.6-cm CHT is localized mainly in the cylindrical part of the channel and beyond the thruster exit, in the plume. The potential variation along the thruster axis between the central ceramic piece and the channel exit is insignificant. Its maximum possible value is within the data spread of the measurements, which is about 25 V. Much larger potential drops along the magnetic field lines were observed in the end-Hall ion source [31], which has a mirror-type magnetic field distribution similar to that in the central part of the CHT.

Due to a rather large uncertainty of the plasma density measurements, it was possible to determine only the interval, in which the real value of N_e was located. The variation bars in Fig. 3(c) span between the upper and the lower estimates of N_e obtained in the experiments. Due to the reasons discussed in detail in [27], the real values of the plasma density are believed to be closer to the upper bounds of the corresponding intervals. The plasma density in the 2.6-cm CHT has a prominent peak at the thruster axis: N_e at the axis is 4–8 times larger than in the annular part of the channel. This density elevation at the thruster axis should be, in fact, common to all scaled down Hall thrusters and might lead to the enhanced erosion of the tip of the central ceramic piece.

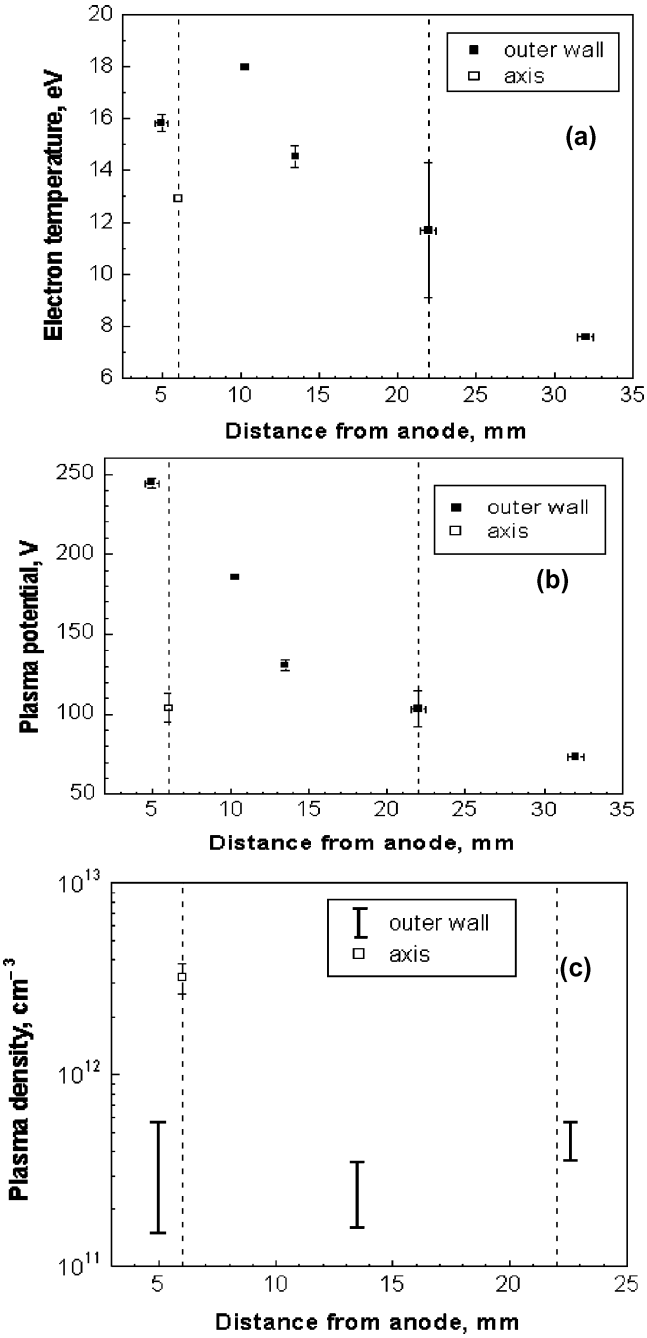

Fig. 3. (a) Electron temperature, (b) plasma potential, and (c) plasma density profiles in the 2.6-cm CHT [28]. Dashed lines at $z = 6$ mm and $z = 22$ mm show the edge of the annular channel part and the thruster exit, respectively. In (a) and (b), Y axis error bars represent the entire statistical spread of the measured data. For plasma density measurements near the outer channel wall (c), only the intervals, in which the real values of the plasma density are located, can be given.

III. Numerical Simulations

The MC code, developed to study the electron dynamics in the thruster channel, is described in detail elsewhere [28]. In the present paper, we only outline the main code's features and show the major results of the numerical simulations.

A. Modeling Approach and Assumptions

The MC code in the present realization is used to simulate the charged particles dynamics in the channel of the 2.6-cm CHT. The particle trajectories are traced in the given electric and magnetic fields, which are assumed to be azimuthally symmetric. The magnetic field distribution for a given arrangement of the magnetic circuit is simulated using the commercially available Field Precision software [32].

The electric field distribution is obtained from the experiments assuming that the magnetic field surfaces are equipotential. We assign the measured potential values to the magnetic field lines sampled by the corresponding probes [see Fig. 2(b)]. Between the locations of the probes plasma potential $\phi(z, R)$ is assumed to vary linearly with magnetic flux function $\psi(z, R)$, $\phi(z, R) \propto \psi(z, R)$. The anode's surface is equipotential with

$\phi = 250$ V. As suggested by the measurements, the magnetic field line at the thruster axis is assumed to be equipotential as well, and is assigned the potential of 100 V. The sheath potential drop is assumed to be concentrated in the infinitely thin layer near the walls.

In the MC simulations, charged particle trajectories are integrated in three-dimensional (3-D) $3v$ (three dimensions in configuration space, three dimensions in velocity space). Newton's equations of motion are resolved using a modification of the explicit leap-frog scheme by Boris [33]. The time step of integration $\Delta t = 0.1/\omega_c$ was used in simulations, where ω_c is the particle gyrofrequency (for electrons, $\Delta t \sim 3 \times 10^{-12}$ s).

We apply the MC technique [34] to simulate electron collisions, which include collisions with neutral Xe atoms (elastic scattering, excitation, and single ionization), with channel walls [attachment, backscattering, and secondary electron emission (SEE)], and with electric field fluctuations (anomalous or "Bohm" diffusion). For simplicity, the neutral gas density N_a is assumed to be uniform in the entire channel volume, and the near-wall sheath potential drop ϕ_{sh} is assumed to be constant along all the channel walls. To treat MC collisions, the numerically efficient null-collision method [34] is implemented in the code.

Scattering of electrons on the channel walls involves three different processes, namely, true secondary electron emission (SEE), elastic backscattering, and inelastic backscattering. For low primary electron energies, which are typical of Hall thrusters, the energy spectra of true secondary electrons and backscattered electrons merge. Thus, only the total SEE yield $\gamma(\varepsilon)$ is available for the traditional Hall thruster channel materials, such as boron-nitride. Using the approach developed in [10], we split the total SEE yield $\gamma(\varepsilon)$ into true secondary emission yield δ and total backscattering yield η. When an electron that can penetrate the sheath collides with the wall, either electron attachment, or backscattering, or true SEE can occur. The probabilities of these processes can be determined from the values of γ, δ, and η [28].

We imposed the anomalous Bohm conductivity inside the channel in order to account for fluctuation-enhanced electron transport. It was assumed that electrons scatter primarily in the azimuthal fluctuations of the electric field. When an electron undergoes a collision with the electric field fluctuation, the perpendicular, with respect to $\mathbf{B}$, electron velocity component is assumed to scatter isotropically. The parallel velocity component does not change. Thus, the guiding center of the electron orbit gets a random shift in the plane perpendicular to $\mathbf{B}$ on the order of the electron gyroradius. The frequency of Bohm diffusion collisions is assumed to be $\nu_B = \kappa_B \omega_c/16$, where κ_B is a fitting parameter that does not depend on the electron energy. Using the customary approach, we introduce one fitting parameter, κ_B, which is applied to calculation of the anomalous collision frequency in the entire discharge volume. However, in reality, the effective κ_B may vary across the magnetic field [21].

It is worth mentioning that for kilowatt and subkilowatt Hall thrusters most of the models that impose Bohm conductivity in the channel show that the best agreement between the experimental and simulated data is achieved when κ_B is less than one, on the order of 0.1–0.4 [8], [9], [11]–[16].

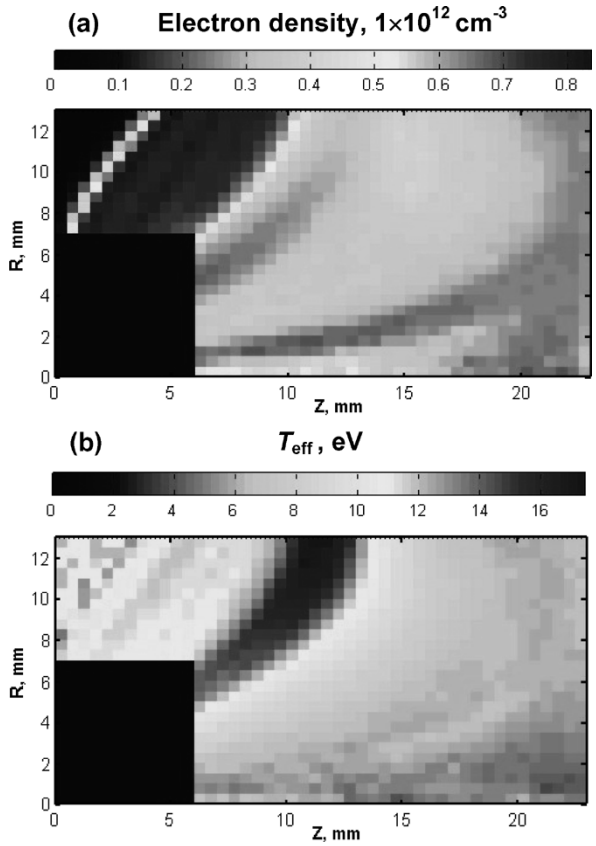

Fig. 4. (a) Distributions of the electron density and (b) the effective electron temperature in the channel of the 2.6-cm CHT. Solid dark rectangle in the lower left-hand side corner of the pictures ($0 < z < 6$, $0 < R < 7$) represents the cross section of the central ceramic piece.

In the electron transport simulations, primary electrons injected from the cathode are assumed to have monoenergetic distribution with $\varepsilon = 20$ eV. Similar energy of electrons injected from the cathode was observed in a low-power conventional Hall thruster [35]. The primary electrons are launched at the thruster exit, with a uniform distribution of the electron flux across the channel cross section. The electron current fraction is taken to be equal to 0.5 (see Section II). The electrons are followed successively one after another until both primary electrons and secondary ones (the latter being generated due to ionization and secondary electron emission from the walls), either reach the anode or get attached to the walls. EDF is determined in $z-R-\varepsilon$ phase space using the approach developed by Boeuf and Marode [36]. Electron density and effective electron temperature are determined as the corresponding moments of the EDF.

B. Numerical Results

The main objective of the performed numerical simulations was to determine what rate of electron cross-field diffusion could explain the observed discharge current. We performed the parametric study of the dependency of plasma parameters distribution on the electron cross-field conductivity. Numerical simulations were carried out for four different values of κ_B, with N_a and ϕ_{sh} chosen according to the experimental constraints [28]. The main results obtained in the simulations can be summarized as follows.

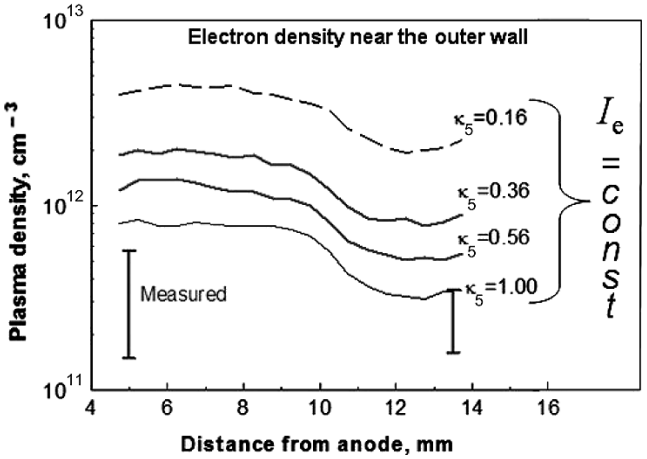

Fig. 5. Calculated profiles of the plasma density at the outer channel wall between $z = 5$ mm and 13.5 cm locations for different values of κ_B. Uncertainty bars represent the results of the plasma density measurements.

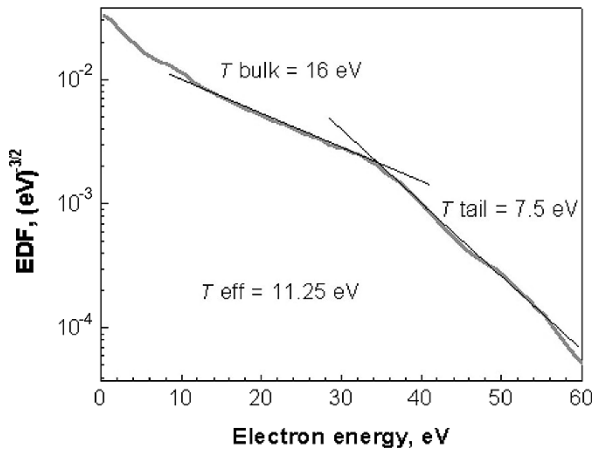

Fig. 6. Typical electron distribution function (EDF) in the annular part of the channel. $T_{\rm bulk}$ and $T_{\rm tail}$ are obtained by fitting the corresponding parts of the EDF with linear functions.

The distributions of the electron density N_e and effective electron temperature $T_{\rm eff}$ obtained in simulations are shown in Fig. 4. Note that the maximum electron density is achieved in the annular part of the channel. Although there is a slight elevation of N_e at the thruster axis, its value, as opposed to the results of the experiments, is lower than the density in the annular part of the channel. The plasma density spike observed at the thruster axis [see Fig. 3(c)] might be due to the convergent ion flux [37]. When κ_B is varied, the distribution of the electron density in the channel remains similar to that shown in Fig. 4(a), with the characteristic magnitude of N_e decreasing when κ_B is increased. For different values of κ_B, the distributions of $T_{\rm eff}$ remain very similar to each other.

When the parameter κ_B is increased, the electron density required to conduct the observed discharge current becomes smaller. This fact is illustrated in Fig. 5, where the axial profiles of N_e near the outer channel wall are plotted for different values of κ_B. As the rate of cross-field electron diffusion approaches the Bohm value $\kappa_B = 1$ [38], the electron density at $z = 5$ mm and 13.5 mm gets almost equal to the measured plasma density. As mentioned herein, the real values of the plasma density are believed to be closer to the upper bounds of the corresponding uncertainty bars in Fig. 5. Even though the match between the measured and simulated values of N_e is not perfect, the trend of N_e dependency on κ_B is evident.

The present model is not expected to give a correct quantitative description of the EDF variation along the thruster channel. However, the general shape of the EDF obtained in our simulations appears to be in a good qualitative agreement with the results of work [20], where the EDF in the Hall thruster channel was determined by solving the electron Boltzman equation.

A typical EDF in the annular part of the channel is shown in Fig. 6. The EDF averaging is performed in order to get statistically more ample phase space data. As can be concluded from Fig. 6, electron–wall collisions deplete the tail of the EDF. The resultant shape of the EDF appears to be bi-Maxwellian. Recent kinetic simulations [39] that focused on the problem of plasma–wall interaction in Hall thrusters showed that the EDF is not only depleted at high energy, but also strongly anisotropic and nonmonotonic. In the given distribution of electric field, Bohm parameter κ_B governs the rate of electron thermal energy pumping. As κ_B (and, consequently, ν_B) decreases, the tail of the distribution function gradually weakens. For $\kappa_B = 1$ (as in Fig. 6), the ratio of the bulk and the tail electron temperatures is approximately equal to 2.1. For $\kappa_B = 0.16$, this ratio increases to 3.3, while the effective electron temperature remains approximately the same as in $\kappa_B = 1$ case. In the cylindrical part of the channel, where the electron–wall collision frequency is smaller, the influence of the walls on the EDF shape is less pronounced.

IV. Discussion

In view of Fig. 5, in order to explain the observed plasma density, the electron anomalous collision frequency ν_B should be high, on the order of the Bohm value $\nu_B \sim \omega_c/16$ ($\kappa_B = 1$). This conclusion can be supported also by the following argument concerning electron current conduction in the annular part of the channel. The magnetic field in the annular part of the 2.6-cm CHT is mainly radial. The average value of the magnetic field at the median is about 650 G. At $z = 5$ mm, where the closest to the anode probe was located in the experiments, the axial electric field E is about 110 V/cm. We can estimate the average electron velocity in the axial direction U_e as $U_e = \kappa_B Ee/(16m\omega_c) \sim 1.06\kappa_B \times 10^6$ cm/s. Now, we note that in the 2.6-cm CHT the fraction of the discharge current carried by the ions varies from essentially zero at the anode ($I_I \ll I_e$) to about 0.5 at the thruster exit ($I_I \approx I_e \approx I_d/2$). Taking in to account that the overall potential drop in the annular part of the channel is not large, we conclude that the electron current in the annular part of the channel should be at least a few times larger than the ion current. Thus, in the annular part of the channel $I_e \approx I_d \approx eN_eS_aU_e$, where $S_a = 3.77$ cm^2 is the anode area. Therefore, we can relate the plasma density required to conduct the observed current ($I_d = 0.6$ A) to the rate of electron cross-field transport

$$N_e \sim \frac{9.4}{\kappa_B} \times 10^{11}\text{cm}^{-3}. \tag{2}$$

For $\kappa_B = 1$, the value of N_e acquired from this rather crude estimate, $N_e = 9.4\times10^{11}$ cm^{-3}, is in a good agreement with the

result of simulations, $N_e = 8.2 \times 10^{11}$ cm^{-3}. More importantly, the values of N_e obtained in simulations for different values of κ_B follow $1/\kappa_B$ scaling quite well, as illustrated in Fig. 7.

It is important to mention that the value of parameter κ_B, which, for the low-power CHT, gives the best agreement between the simulations and experiments ($\kappa_B \sim 1$), is a few times larger than those obtained typically in the modeling of conventional Hall thrusters ($\kappa_B \sim 0.1 - 0.4$) [8], [9], [11]–[16]. Thus, the rate of electron fluctuation-enhanced diffusion, which is required to explain the discharge current observed in the CHT, should be higher than that in conventional Hall thrusters. The anomalous electron transport in the CHT is believed to be induced by high-frequency plasma instabilities [40], [41]. Interestingly, in the frequency range below ~100 kHz, the 2.6-cm CHT operates quieter than the annular Hall thruster of the same size [25].

The electron–wall collisions make an insignificant contribution to the electron current conduction, as compared with the fluctuation-induced electron scattering. For the parameters of Fig. 6, the average electron–wall collision frequency ν_{ew} is approximately equal to 1×10^7 s^{-1}, while the anomalous collision frequency averaged along the corresponding field line is about 7.2×10^8 s^{-1} [28]. At the same time, the total electron-atom collision frequency ν_{ea} is on the order of 2.4×10^7 s^{-1}. Thus, $\nu_{ew} \leq \nu_{ea} \ll \nu_B$. Both the electron–wall and the electron–atom collision frequencies decrease toward the thruster exit. The inequalities $\nu_{ew}, \nu_{ea} \ll \nu_B$ are satisfied throughout the channel. In the real thruster, the neutral gas density decreases toward the channel exit due to ionization and the effective channel widening upon the transition from the annular to the cylindrical channel part. If a realistic neutral gas density profile was used in the simulations, ν_{ew} would become larger than ν_{ea} in the cylindrical part of the channel. However, in order to explain the observed discharge current, the anomalous collision frequency ν_B would have to remain much larger than both ν_{ew} and ν_{ea}.

Even though the electron–wall collisions appear to have little effect on the electron cross-field transport, the electron–wall interaction is very important in terms of electron energy balance [42], [43]. For the parameters of Fig. 6, for example, the electron energy loss at the walls q_{ew} is equal to about 9.7 J/cm^3, while the energy loss due to inelastic electron–atom collisions q_{ea} is about 4.9 J/cm^3. q_{ew} and q_{ea} both decrease toward the channel exit and have values comparable with each other. The conclusions concerning the electron cross-field transport seem, however, to be insensitive to the details of the electron energy balance.

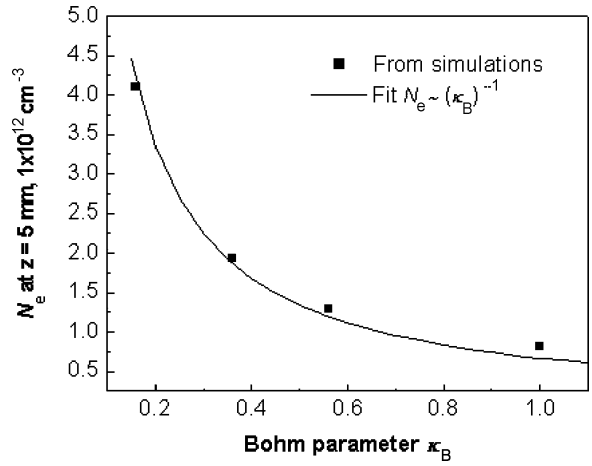

Fig. 7. Simulated values of N_e at $z = 5$ mm near the outer wall versus Bohm parameter κ_B. Solid line shows the result of fitting the simulated data with function A/κ_B.

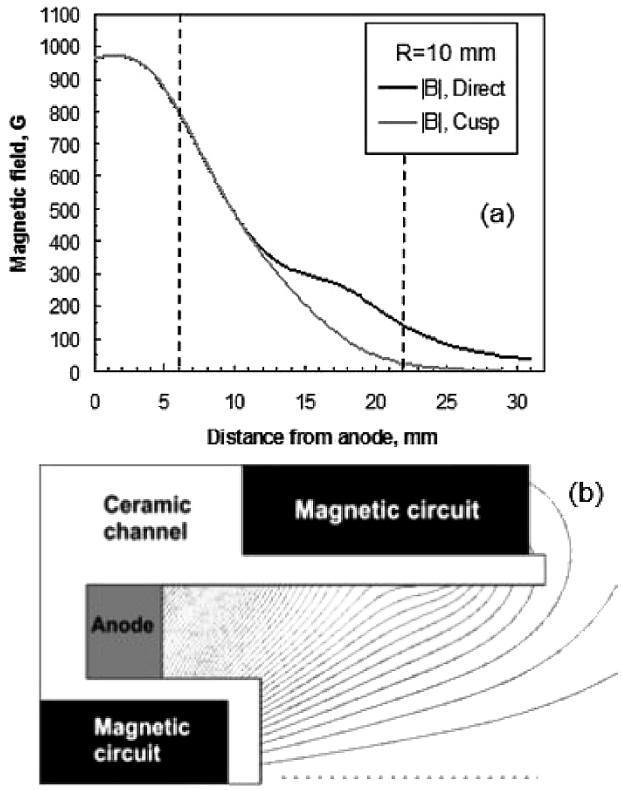

Fig. 8. (a) Magnetic field profiles in the 2.6 cm CHT in the "direct" ($I_{\rm back} = 2.5$ A, $I_{\rm front} = 1$ A) and "cusp" ($I_{\rm back} = 2.5$ A, $I_{\rm front} = -1$ A) configurations. Dashed lines at $z = 6$ mm and $z = 22$ mm show the edge of the annular channel part and the thruster exit, respectively. (b) Magnetic field lines in the "direct" configuration for the same coil currents as in Fig. 8(a) (compare with Fig. 2(b), where the field lines in the "cusp" configuration are shown).

V. Recent Experimental Results and Plans for Future Work

The effect of the magnetic field on the discharge characteristics and efficiency of the low-power CHTs with channel outer diameters of 2.6 and 3 cm was investigated recently [25], [44]. In this section, we briefly describe a few interesting results obtained in these experiments. The observed effects (even though the underlying physics remains largely unexplored) have important implications for the problem of electron cross-field transport and suggest the directions for further studies.

The variation of the current in the back magnetic coil of the CHT mainly changes the magnetic field magnitude without altering the shape of magnetic field surfaces. It is generally observed that the increase of the back coil current leads to the monotonic decrease of the discharge current. The variation of

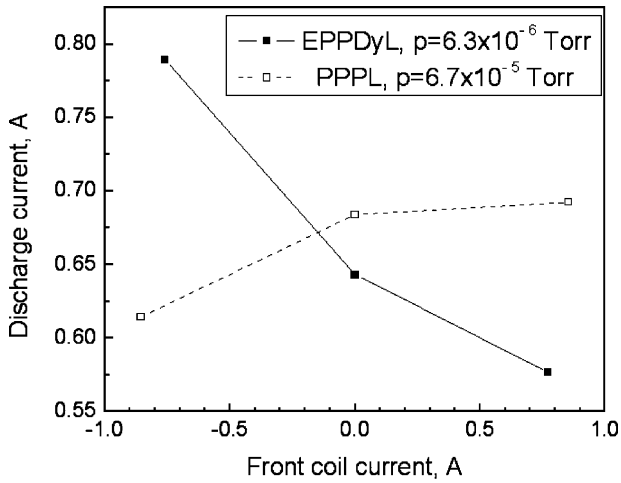

Fig. 9. Dependences of the discharge current on the current in the front magnetic coil in the 2.6-cm CHT for the EPPDyL and PPPL facilities. All discharge parameters are the same (anode flow rate $\mu = 0.4$ mg/s, $U_d = 250$ V, $I_{\rm back} = +3$ A), except for the background gas pressure, which is equal to 6.3×10^{-6} torr for the EPPDyL tank and 6.7×10^{-5} torr for the PPPL tank.

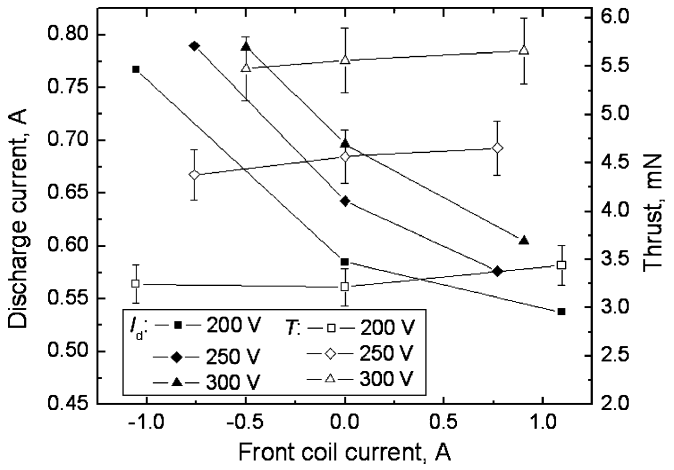

Fig. 10. Dependencies of the discharge current and thrust on the front coil current in the 2.6-cm CHT operated in the EPPDyL facility (background gas pressure $\sim 6 \times 10^{-6}$ torr). Anode and cathode xenon flow rates are 4 and 2 sccm, respectively; $I_{\rm back} = 3$ A. $I_{\rm front} > 0$ ($I_{\rm front} < 0$) corresponds to the direct (cusp) magnetic field configuration.

the front coil current changes the shape of the magnetic field surfaces, with the most pronounced changes occurring in the cylindrical part of the channel. When the current in the front coil is counter-directed to that in the back coil ($I_{\rm front} < 0$), the "cusp" magnetic field with an enhanced radial component is created (see Fig. 2). Swapping the polarity of the front coil current ($I_{\rm front} > 0$) leads to the enhancement of the axial component of the magnetic field (see Fig. 8) and generation of a stronger magnetic mirror near the thruster axis. The goal of the performed experiments was to investigate the dependence of the discharge current and generated thrust on the current in the front magnetic coil.

The experiments were performed in the Electric Propulsion and Plasma Dynamics Laboratory (EPPDyL), Princeton University, Princeton, NJ [45]. The operating background pressure of xenon in the EPPDyL vacuum facility was about one order of magnitude smaller than that in the Small Hall Thruster facility at PPPL. Importantly, it was observed that the magnetic field configuration that minimizes the discharge current depends on the background gas pressure in the tank. In Fig. 9, the variation of the discharge current I_d with the current in the front coil $I_{\rm front}$ is shown for the EPPDyL and PPPL facilities. All discharge parameters are the same (anode flow rate $\mu = 0.4$ mg/s, $U_d = 250$ V, $I_{\rm back} = +3$ A), except for the background xenon pressure, which is about 6×10^{-6} torr for the EPPDyL tank and 7×10^{-5} torr for the PPPL tank. In the experiments at EPPDyL, when the background gas pressure in the near-filed thruster plume was raised by increasing xenon flow rate to the cathode, the values $I_d(I_{\rm front})$ were found to shift closer to those corresponding to the PPPL conditions. It is important to emphasize, however, that electrons in the plume plasma are collisionless in both the PPPL and EPPDyL facilities. The electron mean free path is about the size of the tank, which is much larger than the thruster dimensions.

It is clear form Fig. 9 that the cusp magnetic field configuration minimizes the discharge current at high background pressure, while the direct configuration does the same at low pressure. Now, at low background pressure, the increase of $I_{\rm front}$ above $\sim +1$ A leads to the negligible variation of the discharge current. The decrease of $I_{\rm front}$, on the contrary, brings about a rather sharp increase of I_d. Along with it, as the magnetic field configuration is changed from direct to cusp, the generated thrust slightly decreases (see Fig. 10). Consequently, in the voltage range from 200 to 300 V, the anode efficiency in the direct configuration is approximately factor of 1.5–1.7 larger than that in the cusp configuration.

The fact that the discharge current decreases with the increase in $I_{\rm front}$ (see Fig. 10) implies that the electron transport to the anode is suppressed more strongly in the direct magnetic field configuration than in the cusp configuration. Indeed, from the data shown in Fig. 10 it follows that

$$I_i^c \sim 0.95 I_i^d \sqrt{\frac{\varepsilon^d}{\varepsilon^c}} \tag{3a}$$

$$I_d^c \sim 1.37 I_d^d. \tag{3b}$$

Here, I_I is the ion current, ε is the mean ion energy, and superscripts d and c refer to the direct and cusp polarities, respectively. From (3), we obtain the ratio of the electron currents in the cusp and direct configurations

$$\frac{I_e^c}{I_e^d} \approx 1.37 + \frac{I_i^d}{I_e^d}\left(1.37 - 0.95\sqrt{\frac{\varepsilon^d}{\varepsilon^c}}\right). \tag{4}$$

When the thruster magnetic field configuration is changed, it is very unlikely that the average ion energy varies by more than about factor of 2. Thus, the ratio I_e^c/I_e^d is about 1.3–1.5.

The fact that the electron current in the direct configuration is smaller does not necessarily imply that the rate of electron cross-field transport is smaller. Plasma measurements, similar to those described in Section II, are required to understand how the magnetic field configuration and background gas pressure influence the electron anomalous transport. Studying the dependence of the plasma parameters on the magnetic field and gas pressure is a subject of ongoing research.

VI. Conclusion

Scaling to low-power Hall thrusters requires the magnetic field to be increased inversely with length, as the thruster channel size is decreased. In a strong magnetic field of a low-power Hall thruster, the rate of electron cross-field diffusion, required to sustain the discharge, can differ from that in a Hall thruster operating in the conventional kilowatt or sub-kilowatt power range. Thus, understanding of the mechanisms of electron transport is essential for the development of higher efficiency low-power thrusters and for scaling to small sizes.

The conventional (annular) Hall thrusters become inefficient when scaled to small sizes because of the large surface-to-volume ratio and the difficulty in miniaturizing the magnetic circuit. Also, the erosion of the walls of a small annular channel can severely limit the thruster lifetime. An alternative approach, which may be more suitable for scaling to low power, is a CHT. The 9-cm CHT, operated in the sub-kilowatt power range, and the miniature 2.6- and 3-cm CHT, operated in the power range 50–300 W, exhibit performance comparable with the conventional state-of-the-art annular Hall thrusters of the same size. Ion acceleration in the CHTs occurs mainly in the cylindrical part of the channel and beyond the thruster exit. Thus, CHTs, having lower surface-to-volume ratio as compared with conventional annular design Hall thrusters, should suffer lower erosion of the channel walls and, therefore, have a longer lifetime.

Plasma potential, ion density, and electron temperature profiles were measured inside the 2.6-cm cylindrical Hall thruster, operated in the vacuum facility with a relatively high background gas pressure ($< 10^{-4}$ torr). The electron cross-field transport was studied for the typical operating regime. To analyze electron dynamics in the channel region of the 2.6-cm CHT, a Monte Carlo code was developed. The numerical model takes into account elastic and inelastic electron collisions with atoms, electron–wall collisions (backscattering, attachment, and secondary electron emission), and Bohm diffusion. The comparison of numerical and experimental results shows that in order to explain the discharge current, observed in the 2.6-cm CHT, the electron anomalous collision frequency ν_B has to be high. As opposed to most of the conventional Hall thruster models, which predict the ratio ν_B/ω_c to be on the order of 10^{-2}, we find that in the 2.6 cm CHT ν_B has to be on the order of the Bohm value, $\nu_B \sim \omega_c/16$. The anomalous cross-field electron transport in the CHT is believed to be induced by high-frequency plasma instabilities. The EDF in a Hall thruster is depleted at high energy due to electron loss at the walls, thus indicating that the contribution of secondary electrons to cross-field transport is likely insignificant.

The effect of the magnetic field on the discharge current and generated thrust in the 2.6- and 3-cm CHTs was studied in the experiments performed at low background gas pressure ($< 10^{-5}$ torr). These experiments demonstrated that the optimal regimes of thruster operation at low background pressure are, in fact, different from those at higher pressure. For instance, for both the 2.6- and 3-cm CHTs the discharge current decreases and the generated thrust slightly increases as the magnetic field configuration is changed from cusp to direct. This, most likely, implies that the electron transport to the anode is suppressed more strongly and the directionality of ion acceleration is better in the direct magnetic field configuration than in the cusp configuration. The thruster efficiency is accordingly larger in the direct configuration. Future experiments will address the question of how the rate of electron cross-field transport depends on the magnetic field configuration, channel geometric parameters, and the background gas pressure in the tank.

Acknowledgment

The authors are grateful to Prof. E. Choueiri for the provided opportunity to work with the EPPDyL thrust stand, and to R. Sorenson for his assistance in the thrust measurements.

References

[1] I. Morozov and V. V. Savelyev, *Review of Plasma Physics*, B. B. Kadomtsev and V. D. Shafranov, Eds. New York: Consultants Bureau, 2000, vol. 21, p. 203.

[2] J. Mueller, *Micropropulsion for Small Spacecraft, Progress in Astronautics and Aeronautics*, M. M. Micci and A. D. Ketsdever, Eds. Reston, VA: AIAA Progress Astronautics Aeronautics, 2000, vol. 187, p. 45.

[3] A. Fruchtman, "Limits on the efficiency of several electric thruster configurations," *Phys. Plasmas*, vol. 10, no. 5, pp. 2100–2107, 2003.

[4] G. S. Janes and R. S. Lowder, "Anomalous electron diffusion and ion acceleration in a low-density plasma," *Phys. Fluids*, vol. 9, no. 6, pp. 1115–1123, 1966.

[5] A. I. Morozov and V. V. Savel'ev, "Theory of the near-wall conductivity," *Plasm. Phys. Rep.*, vol. 27, no. 7, pp. 570–575, 2001.

[6] A. I. Bugrova, A. I. Morozov, and V. K. Kharchevnikov, "Eexperimental investigation of near wall conductivity," *Sov. J. Plasma Phys.*, vol. 16, no. 12, pp. 849–856, 1990.

[7] E. Fernandez and M. A. Cappelli, "Modeling anomalous electron transport in 2-D simulations of Hall thrusters," *Bull. Amer. Phys. Soc.*, vol. 45, no. 7, p. 166, 2000.

[8] A. Cohen-Zur, A. Fructman, J. Ashkenazy, and A. Gany, "Analysis of the steady-state axial flow in the Hall thruster," *Phys. Plasmas*, vol. 9, no. 10, pp. 4363–4374, 2002.

[9] L. Dorf, V. Semenov, and Y. Raitses, "Anode sheath in Hall thrusters," *Appl. Phys. Lett.*, vol. 83, no. 13, pp. 2551–2553, 2003.

[10] S. Barral, K. Makowski, Z. Peradzynski, N. Gascon, and M. Dudeck, "Wall material effects in stationary plasma thrusters. II. Near-wall and in-wall conductivity," *Phys. Plasmas*, vol. 10, no. 10, pp. 4137–4152, 2003.

[11] E. Ahedo, J. M. Gallardo, and M. Martinez-Sanchez, "Effects of the radial plasma-wall interaction on the Hall thruster discharge," *Phys. Plasmas*, vol. 10, no. 8, pp. 3397–3409, 2003.

[12] M. Keidar, I. D. Boyd, and I. I. Beilis, "Plasma flow and plasma-wall transition in Hall thruster channel," *Phys. Plasmas*, vol. 8, no. 12, pp. 5315–5322, 2001.

[13] J. Bareilles, G. J. M. Hagelaar, L. Garrigues, C. Boniface, J. P. Boeuf, and N. Gascon, "Critical assessment of a two-dimensional hybrid Hall thruster model: Comparisons with experiments," *Phys. Plasmas*, vol. 11, no. 6, pp. 3035–3046, 2004.

[14] J. M. Fife, "Hybrid-PIC modeling and electrostatic probe survey of hall thrusters," Ph.D. dissertation, MIT, Cambridge, 1998.

[15] J. J. Szabo, "Fully Kinetic Numerical Modeling of a Plasma Thruste," Ph.D. dissertation, MIT, Cambridge, 2001.

[16] Y. Raitses, D. Staack, M. Keidar, and N. J. Fisch, "Electron-wall interaction in Hall thrusters," *Phys. Plasmas*, vol. 12, p. 057 104, 2005.

[17] O. Batishchev and M. Martinez-Sanchez, "Charged particles transport in the Hall effect thruster," in *Proc. 28th Int. Electric Propulsion Conf.*, Toulouse, France, 2003, IEPC 03-188.

[18] J. C. Adam, A. Heron, and G. Laval, "Study of stationary plasma thrusters using two-dimensional fully kinetic simulations," *Phys. Plasmas*, vol. 11, no. 1, pp. 295–305, 2004.

[19] L. Jolivet and J. F. Roussel, "Effects of the secondary electron emission on the sheath phenomenon in a hall thruster," in *Proc. 3rd Spacecraft Propulsion Conf.*, Cannes, France, 1999, pp. 367–376.

[20] N. B. Meezan and M. A. Cappelli, "Kinetic study of wall collisions in a coaxial Hall discharge," *Phys. Rev. E, Stat. Phys. Plasmas Fluids Relat. Interdiscip. Top.*, vol. 66, p. 036 401, 2002.
[21] N. B. Meezan, W. A. Hargus, and M. A. Cappelli, "Anomalous electron mobility in a coaxial Hall discharge plasma," *Phys. Rev. E, Stat. Phys. Plasmas Fluids Relat. Interdiscip. Top.*, vol. 63, p. 026 410, 2001.
[22] M. Stanojevic, M. Cercek, T. Gyergyek, and N. Jelic, "Interpretation of a planar Langmuir probe current-voltage characteristic in a strong magnetic field," *Contrib. Plasma Phys.*, vol. 34, no. 5, pp. 607–633, 1994.
[23] V. Khayms and M. Martinez-Sanches, *Micropropulsion for Small Spacecraft, Progress in Astronautics and Aeronautics*, M. M. Micci and A. D. Ketsdever, Eds. Reston, VA: American Inst. Aeronautics Astronautics, 2000, vol. 187, p. 45.
[24] Y. Raitses and N. J. Fisch, "Parametric investigations of a nonconventional Hall thruster," *Phys. Plasmas*, vol. 8, no. 5, pp. 2579–2586, 2001.
[25] A. Smirnov, Y. Raitses, and N. J. Fisch, "Parametric investigation of miniaturized cylindrical and annular Hall thrusters," *J. Appl. Phys.*, vol. 92, no. 10, pp. 5673–5679, 2002.
[26] ——, "Enhanced ionization in the cylindrical Hall thruster," *J. Appl. Phys.*, vol. 94, no. 2, pp. 852–857, 2003.
[27] ——, "Plasma measurements in a 100 W cylindrical Hall thruster," *J. Appl. Phys.*, vol. 95, no. 5, pp. 2283–2292, 2004.
[28] ——, "Electron cross-field transport in a low power cylindrical Hall thruster," *Phys. Plasmas*, vol. 11, no. 11, pp. 4922–4933, 2004.
[29] ——, "The effect of magnetic field on the performance of low-power cylindrical Hall thrusters," in *28th Int. Electric Propulsion Conf.*, Princeton, NJ, Oct. 2005, IEPC paper 2005-099.
[30] K. A. Polzin, T. E. Markusic, B. J. Stanojev, A. Dehoyos, Y. Raitses, A. Smirnov, and N. J. Fisch, "Performance of a low-power cylindrical Hall thruster," in *Proc. 28th Int. Electric Propulsion Conf.*, Princeton, NJ, Oct. 2005, IEPC paper 2005-011.
[31] H. R. Kaufman, R. S. Robinson, and R. I. Seddon, "End-Hall ion source," *J. Vac. Sci. Technol. A*, vol. 5, no. 4, pp. 2081–2084, 1987.
[32] Field Precision. BStat 5.0., Albuquerque, NM. [Online]. Available: http://www.fieldp.com
[33] J. P. Boris, "Relativistic plasma simulation—optimization of a hybrid code," in *Proc. 4th Conf. Num. Sim. Plasmas*, Washington, DC, Nov. 2–3, 1970, pp. 3–67.
[34] C. K. Birdsall, "Particle-in-cell charged-particle simulations, plus Monte Carlo collisions with neutral atoms, PIC-MCC," *IEEE Trans. Plasm. Sci.*, vol. 19, no. 2, pp. 65–85, 1991.
[35] V. Y. Fedotov, A. A. Ivanov, G. Guerrini, A. N. Vesselovzorov, and M. Bacal, "On the electron energy distribution function in a Hall-type thruster," *Phys. Plasmas*, vol. 6, no. 11, pp. 4360–4365, 1999.
[36] J. P. Boeuf and E. Marode, "Monte Carlo analysis of an electron swarm in a nonuniform field: The cathode region of a glow discharge," *J. Phys. D, Appl. Phys.*, vol. 15, no. 11, pp. 2169–2189, 1982.
[37] A. Smirnov, Y. Raitses, and N. J. Fisch, "Electron transport and ion acceleration in a low-power cylindrical Hall thruster," in *Proc. 40th IAA/ASME/SAE/ASEE Joint Propulsion Conf.*, Fort Lauderdale, FL, 2004, AIAA paper 2004-4103.
[38] D. Bohm, *The Characteristics of Electrical Discharges in Magnetic Fields*, A. Guthrie and R. K. Wakerling, Eds. New York: McGraw-Hill, 1949, ch. 2, p. 65.
[39] D. Sydorenko, A. Smolyakov, I. Kaganovich, and Y. Raitses, "Kinetic simulation of secondary electron emission effects in Hall thrusters," *Phys. Plasmas*, vol. 13, p. 014 501, 2005.
[40] E. Y. Choueiri, "Plasma oscillations in Hall thrusters," *Phys. Plasmas*, vol. 8, no. 4, pp. 1411–1426, 2001.
[41] A. A. Litvak, Y. Raitses, and N. J. Fisch, "Experimental studies of high-frequency azimuthal waves in Hall thrusters," *Phys. Plasmas*, vol. 11, no. 4, pp. 1701–1705, 2004.
[42] E. Y. Choueiri, "Fundamental difference between the two Hall thruster variants," *Phys. Plasmas*, vol. 8, no. 11, pp. 5025–5033, 2001.
[43] Y. Raitses, D. Staack, A. Smirnov, and N. J. Fisch, "Space charge saturated sheath regime and electron temperature saturation in Hall thrusters," *Phys. Plasmas*, vol. 12, p. 073 507, 2005.
[44] Y. Raitses, A. Smirnov, and N. J. Fisch, "Cyindrical Hall thrusters," in *Proc. 15th Annu. NASA/JPL/MSFC Adv. Space Propulsion Workshop*, Pasadena, CA, 2004.
[45] E. A. Cubbin, J. K. Ziemer, E. Y. Choueiri, and R. G. Jahn, "Pulsed thrust measurements using laser interferometry," *Rev. Sci. Instrum.*, vol. 68, no. 6, pp. 2339–2346, 1997.

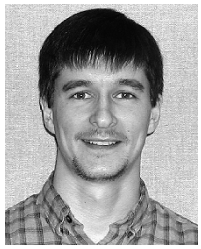

Artem N. Smirnov (S'05) received the M.S. degree in physics from the University of Nizhny Novgorod, Nizhny Novgorod, Russia, in 2000 and the M.S. degree in plasma physics from Princeton University, Princeton, NJ, in 2002.

He is a Graduate Student Research Assistant at Princeton University's Astrophysical Sciences Department, Program in Plasma Physics, carrying out research at Princeton Plasma Physics Laboratory. His research interests are in electric propulsion, low-pressure gas discharge, dusty plasma, and basic plasma diagnostics.

Yevgeny Raitses, photograph and biography not available at the time of publication.

Nathaniel J. Fisch received the B.S., M.S., and Ph.D. degrees in electrical engineering and computer science from the Massachusetts Institute of Technology, Cambridge, where he was an MIT National Scholar, in 1972, 1975, and 1978, respectively.

He is Professor of Astrophysical Sciences and Director of the Program in Plasma Physics at Princeton University, Princeton, NJ. He also is Associate Director for Academic Affairs and Head of the Hall Thruster Laboratory at the Princeton Plasma Physics Laboratory. At Princeton University, he is also an Associated Faculty in the Department of Mechanical and Aerospace Engineering. He is best known for predicting new ways to drive electric current in hot, magnetized plasma by means of electromagnetic waves. In addition to plasma thrusters and related plasma devices, his current research interests include plasma-based methods of generating extreme laser intensities and fusion concepts employing magnetically or inertially confined plasma.

Prof. Fisch received the 2005 James Clerk Maxwell Prize of the American Physical Society, the Ernest Orlando Lawrence Award in 2004, the Department of Energy Bronze Medal for Outstanding Mentor in 2002, and the American Physical Society Award for Excellence in Plasma Physics in 1992. A Fellow of the American Physical Society and a Fellow of the NASA Institute for Advanced Concepts, he received a Guggenheim Fellowship in 1985. In 1998, he was the Chair of the Division of Plasma Physics of the American Physical Society.